Available online at www.sciencedirect.com
ScienceDirect
Journal of the European Ceramic Society 31 (2011) 1431–1438
www.elsevier.com/locate/jeurceramsoc

Quantification of microstructural features in gadolinia-doped ceria containing co-additives by digital image analysis

A.L. Horovistiz *, E.N.S. Muccillo

Energy and Nuclear Research Institute-CCTM, P.O. Box 11049, S. Paulo, SP 05422-970, Brazil

Received 17 October 2010; received in revised form 2 February 2011; accepted 14 February 2011

Abstract

A digital image processing and analysis method has been developed to evaluate the microstructural features of chemically synthesized gadolinia-doped ceria powders containing small amounts of co-dopants. The effects of particles/clusters size, porosity and grain size distribution were examined in detail and compared to those parameters of the standard composition without co-dopants. In addition, the effect of the co-dopants in the grain growth was clarified. Sr^{2+} and Bi^{3+} act as sintering aid for densification of the standard composition. The lowest mean grain size along with higher fraction of porosity was obtained for Na^{+} addition.

Keywords: Grain size; Microstructure-final; Porosity; CeO_2; Digital image processing

1. Introduction

Information on microstructural features of ceramic materials is essential to select suitable sintering conditions, to optimize their thermo-mechanical performance, to suppress negative effects of microstructural defects on relevant properties, and/or to design optimized microstructural features for prospective applications. These relationships are quite obvious in the fields of electroceramics, and those where ceramics with strict mechanical requirements are desired. Typical examples include sintering at relatively low temperatures to prevent high temperature degradation, to enhance the mechanical properties by retaining sub-micrometer grain sizes[1] or to explore unique properties of nanomaterials. The dependence of electrical properties on microstructural features of ceramic materials is also the basis of methods proposed to monitor the sintering behavior by electrical measurements.[2] Some important properties of ceramic materials may be dependent not only on porosity, and microstructural features such as the grain size and pore size distributions, grain shape and its distribution are also relevant. A demonstration on the role of grain shape on the electrical behavior was reported in the literature.[3] Moreover, it is well known that the choice of the starting powder can have a significant influence on the sinterability and on the microstructure of ceramic systems. In addition, agglomerates are known to impart a dominant influence on the densification behavior of powder compacts[4–8] screening the effect caused by the particle size distribution.[9,10]

The development of advanced ceramic materials and the widely recognized intrinsic relationship between their properties and microstructure should, thus, rely on robust and reliable techniques of microstructural analysis. This is based on quantitative microscopy supported by digital image processing and stereology. Its development is strongly related to hardware evolution and to the availability of softwares for digital image processing and analysis.

Several works[11–14] have reported methods to extract microstructural information from polished surfaces of ceramic materials obtained through quantitative microscopy. This approach has many advantages when compared to other methods, such as reducing the data acquisition time, improving the accuracy and reproducibility, and a perfect linking to new concepts of digital microscopy.

Over the last few years, intensive investigations have been carried out on gadolinia-doped ceria, due to its potential application in intermediate temperature solid oxide fuel cells.[15] One of the main drawbacks of this solid electrolyte is the increase in the electronic conductivity at high temperatures and low oxy-

* Corresponding author. Tel.: +55 1182035843; fax: +11 38169370.
E-mail addresses: horovistiz@cv.ua.pt, ahorow@feg.unesp.br (A.L. Horovistiz).

0955-2219/$ – see front matter © 2011 Elsevier Ltd. All rights reserved.
doi:10.1016/j.jeurceramsoc.2011.02.022

Table 1
Synthesized compositions and corresponding notation.

Sample composition	Notation
$Ce_{0.8}Gd_{0.2}O_{2-\delta}$	CGO
$Ce_{0.8}Gd_{0.19}Ag_{0.01}O_{2-\delta}$	CGOAg1
$Ce_{0.8}Gd_{0.19}Sr_{0.01}O_{2-\delta}$	CGOSr1
$Ce_{0.8}Gd_{0.18}Ag_{0.02}O_{2-\delta}$	CGOAg2
$Ce_{0.8}Gd_{0.18}Sr_{0.02}O_{2-\delta}$	CGOSr2
$Ce_{0.8}Gd_{0.19}Bi_{0.01}O_{2-\delta}$	CGOBi1
$Ce_{0.8}Gd_{0.19}Na_{0.01}O_{2-\delta}$	CGONa1

gen partial pressures. One approach to overcome this effect is the use of a co-dopant. In principle, the co-dopant should be able to increase the electrolytic domain and/or to increase the ionic to electronic conductivity ratio. A number of combined additives have been reported in the literature, and most of them include a second rare earth oxide.[16,17] In this work, gadolinia-doped ceria solid electrolyte with small additions of Sr^{2+}, Ag^{+}, Bi^{3+} and Na^{+} were synthesized by the cation complexation technique and characterized taking into account changes in the microstructure of the solid electrolyte.

The main purpose of this work is to propose a method of characterization to optimize the preparation of gadolinia-doped ceria solid solutions. The method is based on the routines of a public domain digital image processing software: the NIH Image J.[18] This approach consists of the following steps: (1) to obtain the morphological parameters of powders/agglomerates of compositions determined by image analysis, (2) to elaborate a routine of microstructural characterization of sintered samples by digital image processing, (3) to compare the coherence of these data against measurements from other methods, to check the validation of the method.

This method intends to be a useful and costless tool for processing analysis, but it is not proposed as a candidate to substitute any other characterization technique.

2. Material and methods

Cerium nitrate hexahydrate (99.9%, Aldrich), gadolinium oxide (99.9%, Aldrich), and silver nitrate, bismuth carbonate, sodium carbonate and strontium carbonate of reagent grade were used as starting materials. Gadolinia-doped ceria solid solutions were prepared by the cation complexation technique using citric acid as complexant agent. Details of this method of synthesis may be found elsewhere.[19] Co-dopants contents were 1–2 mol%. Gadolinia-doped ceria without co-dopants was also prepared under the same experimental conditions, for comparison purposes. The several prepared compositions and corresponding notation are listed in Table 1.

The initial thermal decomposition of the precursor powder was carried out at 523 K for 1 h (CGO523). After this thermal treatment, the powder still contains a relatively high concentration of carbon residues as revealed by the brownish color. In order to optimize the temperature of calcination, the precursor CGO powder was, subsequently, calcined at 673 K for 15 h (CGO673), 873 K for1 h (CGO873) and 1073 K for 1 h (CGO1073).

After calcination, cylindrical pellets of 10 mm in diameter were prepared by uniaxial pressing at 20 MPa in a steel die followed by isostatic pressing (103 MPa). The sintering of pellets was performed at 1773 K for 3 h in air.

The residual carbon content was determined (CS400, Leco) in calcined powders after addition of a low melting point material. Phase characterization and crystallite size determination were performed by X-ray diffraction, XRD (D8 Advance, Bruker-AXS) using a Ni-filtered Cu K_α radiation in the 20–80° 2θ range. The crystallite size of calcined powders was estimated by the Scherrer equation[20] for (1 1 1), (2 2 0) and (3 1 1) reflections. High-grade silicon powder was used as standard to account for instrument broadening correction. The unit cell parameter, a, and crystallite size were obtained by fitting the diffraction patterns using the FULLPROF[21] software. The Rietveld refinement was performed using a pseudo-Voigt function.

Apparent sintered density of pellets was determined by the Archimedes principle using water as immersing medium.

Microstructural characterization was carried out on polished and thermally etched surfaces of selected pellets by scanning electron microscopy, SEM (XL30, Philips) using secondary electrons. This analysis was intended to register the morphology of powder particles/agglomerates (or clusters), to inspect microstructural defects and to evaluate the grain size distributions and porosity.

3. Image processing

3.1. Morphological analysis and grain size distribution

Sets of images obtained in polished and thermally etched surfaces of different sintered samples were used for grain morphology analysis.

One of the first problems found in digital image processing of the microstructure of relatively porous materials is related to the image itself. In general, the obtained images show grains limited by dark and bright contours involving a gray matrix constituting the background. The software for image analysis do not recognize both bright and dark contours without heavy processing and, then, do not process a reliable estimation of grain size, resulting in larger values for intercept measurements. One solution is to use a sequence of spatial derivative filters and morphological operators to enhance digital images, before calculation of the grain size by an image analyzer. Images of CGOAg1 sample will be used as an example. The overall enhancement process consists of the following steps:

(I) In the original image (Fig. 1a) is applied a convolution by a median filter (Fig. 1b), then this image is gray-level thresholded, and converted to binary scale. The Scharr[22] based derivative filter is applied for the 4 possible directions on copies of original noise-filtered image. After each derivative convolution, the images are filtered again by a 3×3

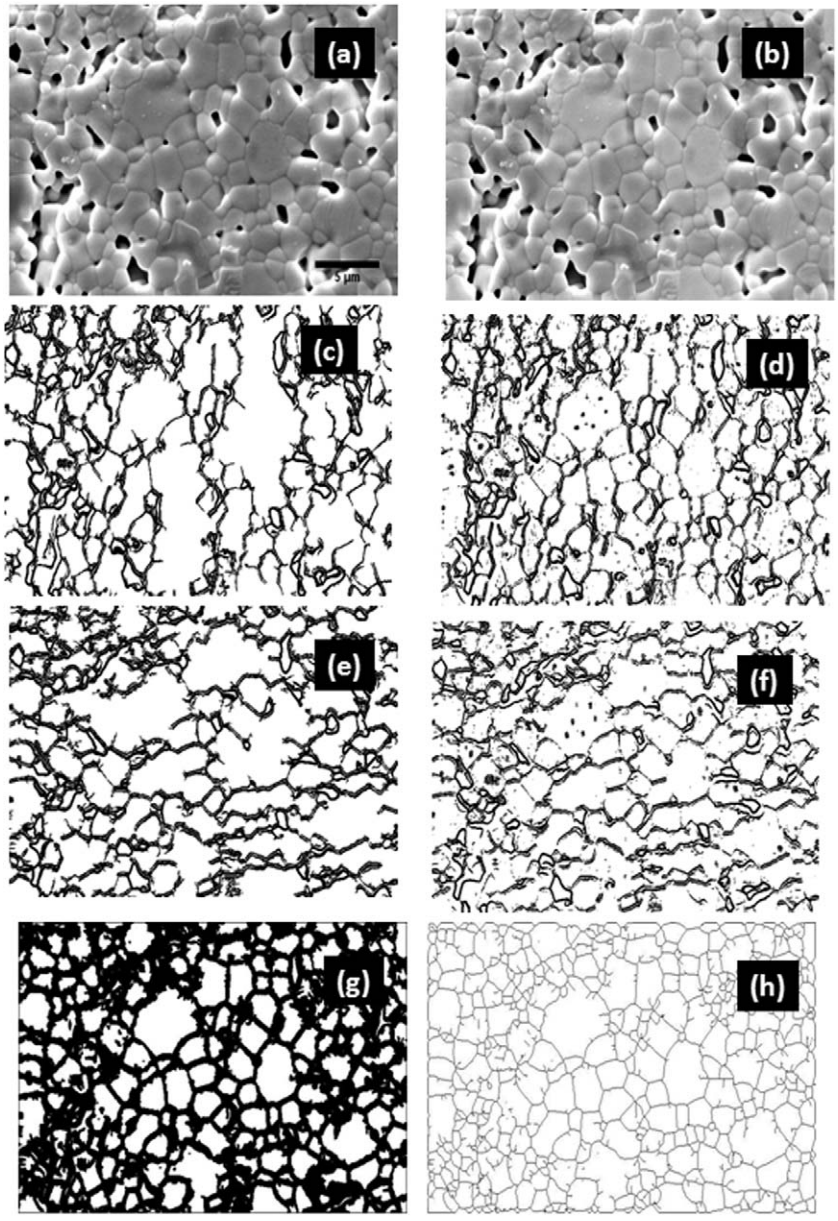

Fig. 1. Example of sequence used for morphological and grain size analysis by digital image processing of polished and etched surface of CGOAg1 sample: (a) original image; (b) shading correction, equalisation and median filtering; (c) thresholding and Sharr at 0°; (d) Sharr at 45°; (e) Sharr at 90°; (f) Sharr at 135°; (g) combination of the four images and derivative filters, erosion and dilation morphological filtering; (h) skeletonization, Fill holes filtering and segmentation by perimeter ratio.

median filter to smooth edges and to suppress residual shot noise (Fig. 1c–f).

(II) The 4 images are added to the same frame, forming a single image with thick and dark contours around grains and a sequence of 10 cycles of successive dilation and erosion morphological operations is performed, using a 3×3 cross structure element (Fig. 1g).

(III) The image is skeletonized and the resulting image is combined by the maximum operation to the original image, and finally a Fill Holes filter is applied (Fig. 1h).

The image analysis and the statistic analysis were performed in a similar way as that reported in Ref. [23].

3.2. Quantification of porosity

In this case, images of CGO sample were taken as an example. The original image (Fig. 2a) was converted to a grayscale image and then thresholded. The connection among edges and pores interfere on the quantification of porosity, therefore, it was applied a morphological segmentation through the filter Watershed followed by a Fill Holes filter (Fig. 2b). Finally, the parameter for shape segmentation called perimeter ratio, PR, is applied. This parameter was defined previously.[23] The definition of PR range was experimentally determined. In this case, only grains presenting PR values inside the range from 0.80 to 1.00 were considered for image analysis. Special

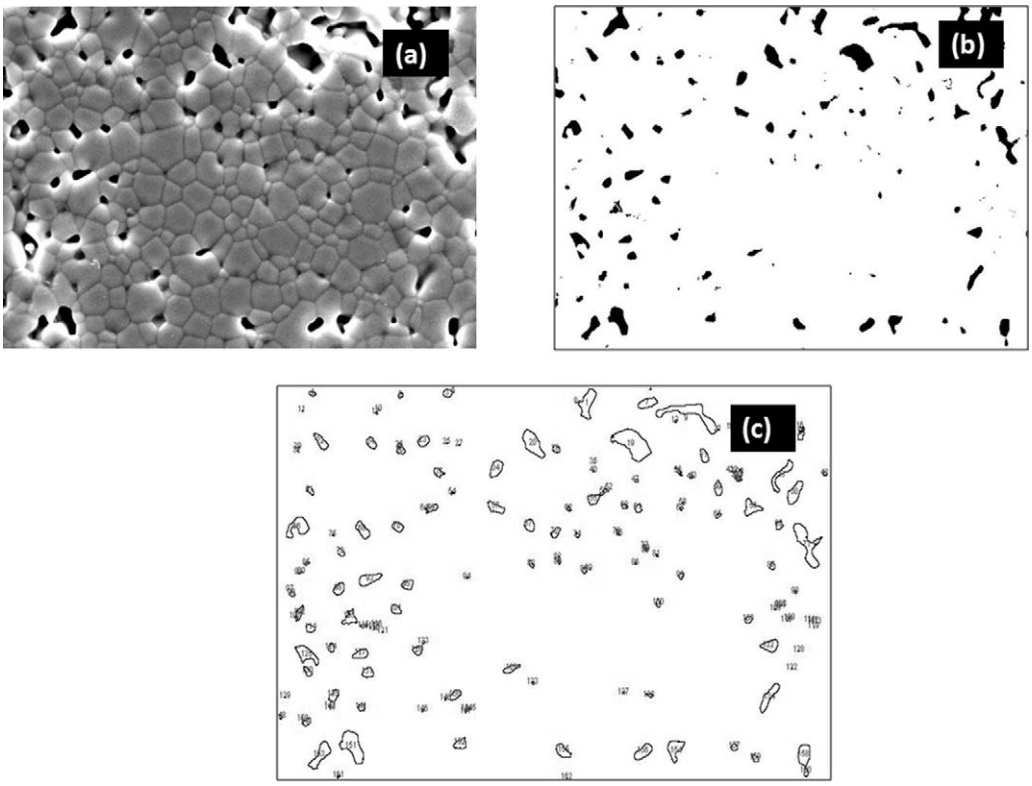

Fig. 2. Example of sequence used for porosity analysis by digital image processing of polished and etched surface from CGO sample: (a) original image; (b) watershed filter and Fill Hole filter; (c) segmentation by perimeter ratio.

care was taken to avoid counting the grains at image borders (Fig. 2c).

4. Results and discussion

4.1. Powder characterization

The calcination route was chosen based on results of X-ray diffraction, analysis of residual carbon contents and inspection of the particle/agglomerate morphology from the scanning electron microscope images.

Fig. 3 shows X-ray diffraction powder patterns of CGO composition calcined at different temperatures. After thermal treatment at 523 K, the powder material is still amorphous to X-rays. Qualitative analysis of the XRD data indicated that all samples exhibited a cubic phase (fluorite-type crystal structure, space group *Fm3m*), as expected. However, these peaks are relatively broad, indicating that the crystallite size is small. The extent of peak broadening decreased with increasing calcination temperature, as shown in Fig. 3. Even after calcination at the highest temperature (1073 K) the peaks remained broad, indicating that the crystallites are still in the nanosize range.

Results of powder refinements are listed in Table 2. The crystallite size increases with the calcination temperature, as expected, and do not greatly differ for different reflections. This increase seems to be approximately linear in the studied temperature range.

Values of the residual carbon content of the CGO powder samples calcined at different temperatures are listed in Table 2. It may be noted a considerable decrease of residual carbon with increasing temperature. The sample CGO673 exhibits high carbon content, although the calcination time, in this case, was longer (15 h).

Fig. 4 shows SEM micrographs of CGO composition calcined at 873 K (a) and 1073 K (b). The evaluation of the size distribution of clusters by digital image processing and analysis is presented in Table 3. The average size of clusters is greater for the powder calcined at 873 K. The reason for this is that with increasing temperature, carbon residues are gradually eliminated. The gas flow generated by the organic by-products across the cluster

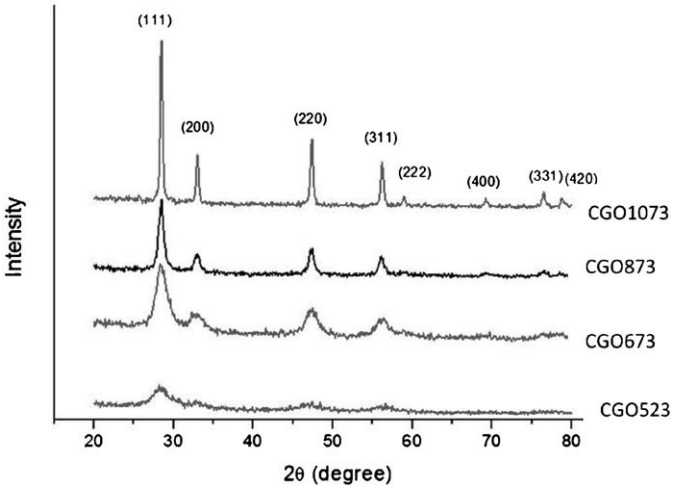

Fig. 3. XRD patterns of CGO powders calcined at different temperatures.

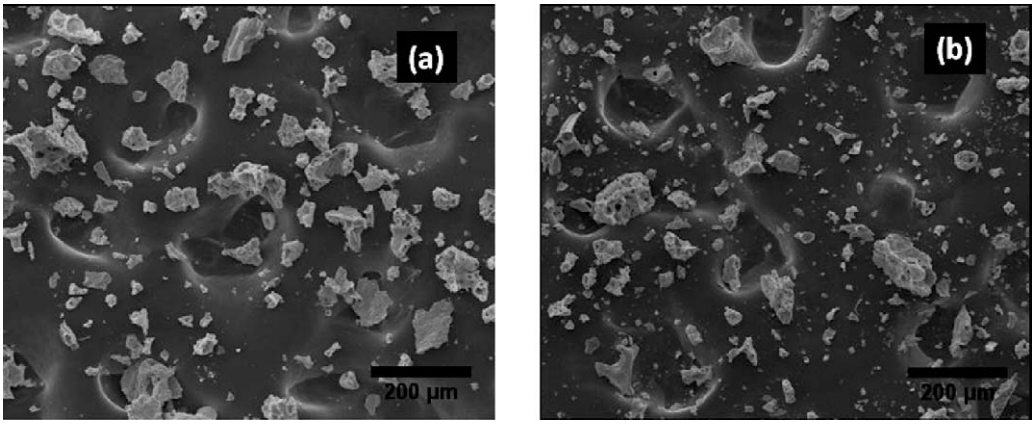

Fig. 4. SEM micrographs clusters in CGO powders calcined at: (a) 873 K for 1 h and (b) 1073 K for 1 h.

Table 2
Values of lattice parameter (*a*), crystallite size for several diffraction peaks, and residual carbon content of CGO samples after calcination under different conditions.

Sample	*a* (Å)	Average size	Carbon content (%)
CGO400	5.428 (2)	5.3	0.41
CGO600	5.4331 (9)	13.6	0.16
CGO800	5.4283 (3)	49.1	0.06

structure leads to "disintegration" of the former clusters. This also explains the porous structure of the clusters. This result is an additional evidence for the use of a relatively high calcination temperature, in order to obtain a more homogeneous particulate material. The analysis of cluster size is of prime importance for ceramic processing of chemically synthesized ceria-based powders. According to Van Herle et al.,[24] the higher is the cluster size the lower is the densification of this type of solid electrolyte. The remaining results were obtained for samples prepared with powders calcined at 1073 K.

Table 4 lists the results of XRD powder refinement for each studied composition after calcination at 1073 K.

The co-dopants modify differently the crystallite size. The introduction of Sr^{2+} decreases the crystallite size, regardless of its content. In contrast, the addition of Ag^{+} tends to increase the crystallite size with increasing the content of the additive. It may be observed that the addition of Bi^{3+} do not change considerably the crystallite size, whereas the addition of Na^{+} resulted in the highest average value of the crystallite size. It is worth to note that Bi^{3+} and Na^{+} have similar ionic radius (1.17 and 1.18 Å, respectively, in 8-fold coordination). The same occurs for Sr^{2+} and Ag^{+} (1.26 and 1.28 Å, respectively). Therefore, from the above results, it may be concluded that the crystallite size of the co-doped ceramics is not primarily influenced by the ionic cation radius.

Table 4
Values of lattice parameter (*a*) and crystallite size for each studied composition after calcination at 1073 K.

Sample	*a* (Å)	Average size (nm)
CGO	5.4299 (3)	44.8
CGOAg1	5.4263 (3)	44.6
CGOAg2	5.4256 (5)	45.5
CGOSr1	5.4262 (3)	33.9
CGOSr2	5.4275 (6)	34.4
CGOBi1	5.4253 (8)	46.1
CGONa1	5.4243 (6)	59.9

Fig. 5 shows SEM micrographs of CGOAg2 (a) and CGOSr2 (b) compositions calcined at 1073 K. These nanopowders are agglomerated with a large distribution in the size of clusters.

The morphological analysis of powders calcined at 1073 K of the two compositions is presented in Table 5. The mean particle diameter of samples containing Sr^{2+} as co-additive is about half that of Ag^{+} co-doped CGO.

The coefficient of variation, CV(*x*), is often used to describe size or shape dispersions. This parameter seems to be particularly interesting because it is a measure of homogeneity (or dispersion). It is a dimensionless number that classify the homogeneity of a distribution function with discrete val-

Table 3
Statistical values of main cluster characterization parameters for CGO samples calcined at 873 K and 1073 K.

Cluster parameter	Statistical parameter	CGO873	CGO1073
Area	Mean (μm^2)	1173.2	877.3
	Standard deviation (μm^2)	1903.7	1856.9
	Coefficient of variation	1.6	2.1
Mean diameter	Mean (μm)	30.1	25.6
	Standard deviation (μm)	24.2	21.6
	Coefficient of variation	0.80	0.84

Table 5
Statistical values of main cluster characterization parameters for CGOAg2 and CGOSr2 samples calcined at 1073 K.

Grain parameter	Statistical parameter	CGOAg2	CGOSr2
Area	Mean (μm^2)	276.9	95.5
	Standard deviation (μm^2)	1192.8	368.9
	Coefficient of variation	4.3	3.8
Mean diameter	Mean (μm)	10.6	5.7
	Standard deviation (μm)	15.5	8.7
	Coefficient of variation	1.5	1.3

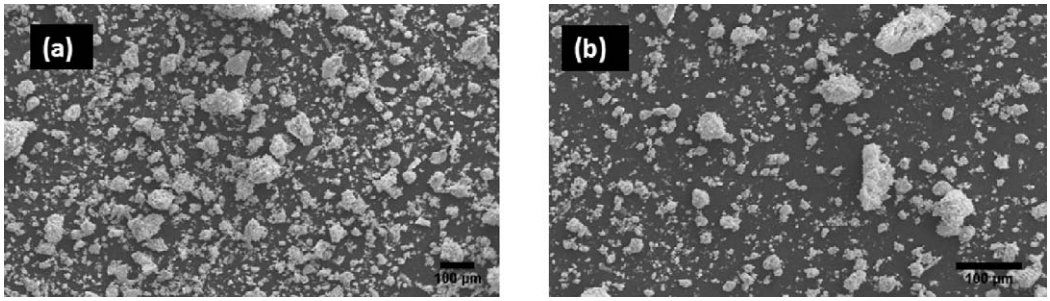

Fig. 5. SEM micrographs of powders calcined at 1073 K for 1 h: (a) GOAg2 and (b) CGOSr2.

ues. Recent works show correlations between size diversity of grains/particles and properties of materials.[25,26] Analysis of CV values in Table 5 shows that the distribution of the particles/clusters is more uniform in CGOSr2 compositions compared to CGOAg2 samples, since the lower coefficient of variation means better homogeneity. These both compositions have particle/cluster distribution more heterogeneous than CGO1073 (Table 3). This suggests that the introduction of Ag and Sr favor the formation of clusters on precursor materials.

4.2. Sintered materials characterization

Fig. 6 shows XRD patterns of CGO and co-doped samples after sintering at 1773 K for 3 h. All these patterns could be indexed according to a single-phase fluorite-type lattice. Diffraction peaks are sharp indicating that high-crystallinity was attained.

The sintered samples are quite dense (relative density between 92% and 97% of the theoretical density value of the CeO_2–Gd_2O_3 solid solution), except for the composition CGONa1 (Table 6). It is worth to note, from this result, that Sr^{2+} and Bi^{3+} improve the densification of CGO. The microstructure of all compositions is shown in the SEM micrographs of Fig. 7, and the results of morphological analysis are summarized in Table 7. Residual porosity, mainly at grain boundaries and at triple junctions may be seen in these micrographs. The average grain size of the standard sample, CGO, is 1.4 μm and remains unchanged, within experimental errors, with additions of Ag^+ and 1 mol% Sr^{2+}. A slight increase of the Sr^{2+} content promoted grain growth. Na^+ was the only co-dopant that reduced the grain size of CGO. Some co-dopants induced changes in porosity. Bismuth, for example, greatly reduces the porosity, whereas sodium promoted a substantial increase in this microstructure feature. Addition of Sr did not change the residual porosity of CGO.

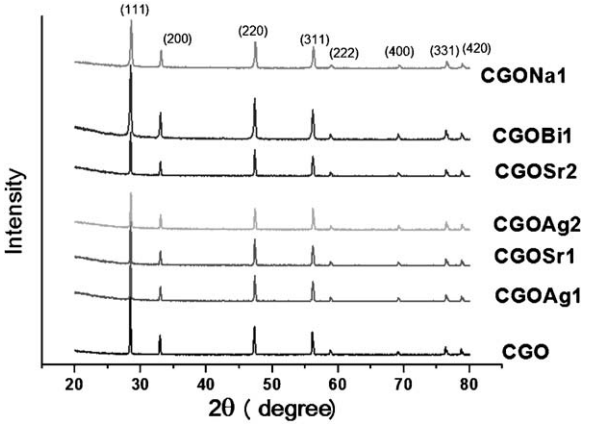

Fig. 6. XRD pattern of studied compositions sintered at 1773 K for 3 h.

There is an evolution of the average grain size with increasing concentration of Sr in solid solution. This gradual grain growth is consistent with the overall results from the refinement of X-ray diffraction, microscopy analysis of the clusters of compositions and the hydrostatic density. There is a clear correlation between the variation of crystallite size (Table 4), the size of clusters (Table 5) and mean values of hydrostatic densities (Table 6) for the compositions with Sr addition. In fact, the CGOSr2 composition exhibits the lowest value of crystallite size along with lower cluster mean diameter and highest density. These effects are most obvious for compositions with 2 mol% of the co-dopant. This set of results suggests that Sr acts primarily as a sintering aid for densification of the CGO solid solution.

The other pair of compositions, CGOBi1 and CGONa1, presents the results of extreme density and pore fraction, respectively. The composition containing Na^+ shows the highest fraction of porosity and lowest hydrostatic density. This composition is more porous than the standard composition CGO. These results also match with the value of crystallite sizes shown in Table 4. In addition, this composition has the lowest value of average grain size. It seems that Na^+ ions do not form solid solution with ceria remaining at the grain boundaries and acting as pinning points, thereby avoiding the growth of grains. However, during the sintering process, sodium ions are removed from the matrix leaving a relatively high fraction of porosity.

Table 6
Values of sintered density of CGO-based compositions.

Composition	Sintered density ($g\,cm^{-3}$)	Relative density of theoretical density (%)
CGO	6.7	92
CGOAg1	6.8	94
CGOSr1	6.9	95
CGOAg2	6.9	95
CGOSr2	6.99	97
CGOBi1	6.95	96
CGONa1	6.2	86

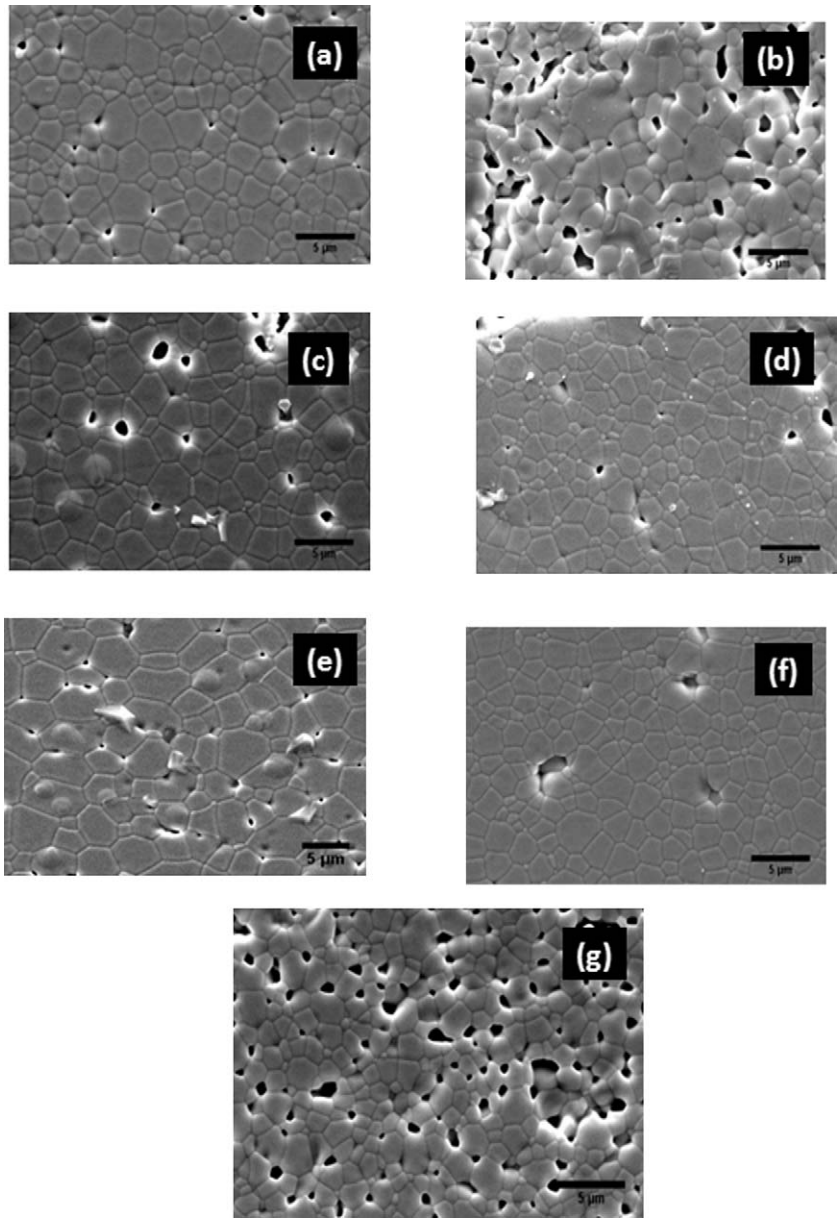

Fig. 7. SEM micrographs of polished and etched surface of studied compositions sintered at 1773 K for 3 h: (a) CGO, (b) CGOAg1, (c) CGOAg2, (d) CGOSr1, (e) CGOSr2, (f) CGOBi1 and (g) CGONa1.

The overall results presented in Table 7 correspond to the combination of information obtained from several microstructures, collected in different fields of each sample in order to compensate for possible heterogeneities. It is important to take into account this heterogeneity indicators and possible consequences for the development of microstructure and its effects on the electrical behavior.

Table 7
Statistical values of main sintered parameters for CGO-based compositions.

Physical parameter	Statistical parameter	CGO	CGOAg1	CGOAg2	CGOSr1	CGOSr2	CGOBi1	CGONa1
Grain area	Mean (μm^2)	1.7	1.3	2.2	1.7	1.8	2.1	0.99
	Standard deviation (μm^2)	1.2	2.5	2.3	1.2	7.3	1.9	0.9
	Coefficient of variation	0.7	1.9	1.1	0.7	0.9	0.9	0.93
Grain mean diameter	Mean (µm)	1.4	1.3	1.4	1.5	2.8	1.7	1.0
	Standard deviation (µm)	0.4	2.5	0.9	0.9	1.4	0.7	1.5
	Coefficient of variation	0.3	1.9	0.6	0.6	0.5	0.5	1.5
Pores	Mean diameter (µm)	0.5	0.8	0.6	0.7	0.3	0.2	0.8
	Porosity (%)	3	7	5	3	3	0.5	12

In effect, there seems to be a relationship between the coefficient of variation and porosity of the material. In general, the more heterogeneous is the composition, the more porous is the system. The discontinuity in the growth of grains, i.e. the heterogeneous distribution of sizes is prone to occur when a small fraction of grains grows much more than the average. A large grain growth at the expense of a thin and uniform matrix, will often display a growth proportional to 1/dm, where dm is the mean grain size of the array. Initially, it was believed that if the mobility of the boundary is the same everywhere, very large grains grow at a much higher rate the larger is its size, producing an enlargement of the size distribution. Recent analysis indicated that relative growth rates are not sufficiently different to explain the extension of the size distribution, once the boundary mobility is the same. Therefore it is concluded that other reasons of local variation in growth rate, such as liquid phases related to eutectic or presence of impurities, non-uniform distribution of porosity, can be invoked to explain this discontinuous grain growth. Another factor may be inhomogeneous packing of the starting powders, leading to local variation in the rate of densification, with regions of rapid densification of agglomerates,[27] subsequently exhibiting a faster grain growth. The analysis of coefficient of variation of Tables 3, 5 and 7 are in general agreement; the CGO nanopowder shows the lower value of CV (Table 3), and the CGOAg2 the highest values (Table 5). The same tendency is followed by the distribution of grain size (Table 7): the more uniform distribution is of CGO samples and the more heterogeneous is that of CGOAG2.

The digital image processing-assisted quantitative analysis of micrographs carried out in this work, provided plenty of data which are fairly important for the purpose of this study.

5. Conclusions

Digital image analysis was used for microstructural characterization of CGO and CGO containing co-dopants powders and sintered samples prepared by the cation complexation technique. The method applied in this work can be extended to other systems. The nanopowders show an agglomerated structure, which varies with the type and content of co-dopants. The crystallite sizes of CGO nanopowders increase with the calcination temperature, whereas the cluster size shows the opposite trend. The average crystallite size of sintered samples decrease with Sr^{2+} and increase with Na^{+} additions. Sr^{2} addition generates lower cluster sizes after calcination than Ag^{+} co-dopant. Bismuth and strontium act as sintering aid for densification of CGO. The mean grain size decreased with Na^{+} co-doping and increased with Ag^{+} addition. The final porosity is higher for Ag^{+} and Na^{+} co-doped samples, and lower for Bi^{3+} containing CGO.

Acknowledgements

The authors would like to acknowledge to Dr. D.D. Khalyavin for helpful comments. This work was supported by FAPESP, CNPq and CNEN. One of the authors (A.L.H.) acknowledges CNPq for the scholarship.

References

1. Zhang TS, Ma J, Kong LB, Hing P, Kilner JA. Preparation and mechanical properties of dense $Ce_{0.8}Gd_{0.2}O_{2-\delta}$ ceramics. *Solid State Ionics* 2004;**167**:191–6.
2. Steil MC, Thevenot F, Kleitz M. Densification of yttria-stabilized zirconia. *J Electrochem Soc* 1997;**144**:390–8.
3. Bouchet R, Knauth P, Laugier JM. Theoretical analysis of the impedance spectra of electroceramics. Part 2: isotropic grain boundaries. *J Electroceram* 2006;**16**:229–38.
4. Baron B, Kumar CS, Le Gonidec G, Hampshire S. Comparison of different alumina powders for the aqueous processing and pressureless sintering of Al_2O_3–SiC nanocomposites. *J Eur Ceram Soc* 2002;**22**:1543–52.
5. Ch'ng HN, Jingzhe P. Sintering of particles of different sizes. *Acta Mater* 2007;**55**:813–24.
6. Kopylov YL, Kravchenko VB, Komarov AA, Lebedeva ZM, Shemet VV. Y_2O_3 nanopowders for laser ceramics Nd. *Opt Mater* 2007;**29**:1236–9.
7. Mæland D, Suciu C, Wærnhus I, Hoffmann AC. Sintering of 4YSZ (ZrO_2 + 4 mol% Y_2O_3) nanoceramics for solid oxide fuel cells (SOFCs), their structure and ionic conductivity. *J Eur Ceram Soc* 2009;**29**:2537–47.
8. Li SP, Lu JQ, Fang P, Luo MF. Effect of powder thermal treatment on the microstructure and electrical properties of doped ceria ceramics. *Mater Lett* 2009;**63**:1689–92.
9. Dell'Agli G, Mascolo G. Sinterability of 8Y–ZrO_2 powders hydrothermally synthesized at low temperature. *Solid State Ionics* 2003;**160**:363–71.
10. Mostafa NY, Characterization. Thermal stability and sintering of hydroxyapatite powders prepared by different routes. *Mater Chem Phys* 2005;**94**:333–41.
11. Kleinlogel CM, Gaukler LJ. Sintering and properties of nanosized ceria solid solutions. *Solid State Ionics* 2000;**245**:567–73.
12. Abrantes JCC, Labrincha JA, Frade JR. Applicability of the brick layer model to describe the grain boundary properties of strontium titanate ceramics. *J Eur Ceram Soc* 2000;**20**:1603–9.
13. Coster M, Arnould X, Chermant JL, Chermant L, Chartier T. The use of image analysis for sintering investigations: the example of CeO_2 doped with TiO_2. *J Eur Ceram Soc* 2005;**25**:3427–35.
14. Boczkowska A, Babski K, Konopka K, Kurzydłowski KJ. Quantitative description of ceramic–elastomer composites with percolation microstructures. *Mater Charact* 2006;**56**:389–93.
15. Steel BCH. Appraisal of $Ce_{1-y}Gd_yO_{2-y/2}$ electrolytes for IT-SOFC operation at 500 °C. *Solid State Ionics* 2000;**129**:95–110.
16. Zha SW, Xia CR, Meng GY. Effect of Gd (Sm) doping on properties of ceria electrolyte for solid oxide fuel cells. *J Power Sources* 2003;**115**:44–8.
17. Tadokoro SK, Muccillo ENS. Effect of Y and Dy co-doping on electrical conductivity of ceria ceramics. *J Eur Ceram Soc* 2007;**27**:4261–4.
18. W.S. Rasband, ImageJ, U.S. National Institutes of Health, Bethesda, MD, USA, http://rsb.info.nih.gov/ij/, 1997–2009.
19. Rocha RA, Muccillo ENS. Synthesis and properties of gadolinium-doped ceria solid solutions for IT-SOFC electrolytes. *Mater Res Bull* 2003;**38**:1979–86.
20. Warren BE. *X-ray diffraction*. New York: Dover; 1990.
21. Rodriguez-Carvajal J. Recent advances in magnetic structure determination by neutron powder diffraction. *Physica B* 1993;**192**:55–69.
22. Jähne B. *Digital image processing: concepts, algorithms and scientific applications*, 4th ed. Berlin: Springer; 1997.
23. Horovistiz AL, Frade JR, Hein LRO. Comparison of fracture surface and plane section analysis for ceramic grain size characterization. *J Eur Ceram Soc* 2004;**24**:619–26.
24. Herle JV, Horita T, Kawada T, Sakai N, Yokokawa H, Dokyia M. Fabrication and sintering of fine yttria-doped ceria powder. *J Am Ceram Soc* 1997;**80**:933–40.
25. Dobosz R, PhD Thesis, Warsaw University of Technology; 2009.
26. Wejrzanowski T, Lewandowska M, Kurzydlowski KJ. Stereology of nanomaterials. *Image Anal Stereol* 2010;**29**:1–12.
27. Ma J, Lim LC. Effect of particle size distribution on sintering of agglomerate-free submicron alumina powder compacts. *J Eur Ceram Soc* 2002;**22**:2197–8.